Multi-Stage Estimation Algorithm for Target Vehicle Trajectory Tracking with Applications to E-Scooter Protection*

Hamidreza Alai and Rajesh Rajamani

Abstract— This paper develops a multi-stage estimation algorithm for use on an e-scooter for target vehicle trajectory tracking. Previously designed observers for vehicle trajectory tracking lacked some essential features such as the ability to handle variable velocity, or stable performance in the presence of uncertainties in the measurements. To overcome these shortcomings, the original model of the non-ego vehicle is translated into three separate models for speed, orientation, and position. Three stable observers are designed for these models which are all shown to be stable and robust to uncertainties, in addition to requiring low computational effort. The new estimation algorithm outperforms previous observers in both simulations and experimental results. The developed observer can be especially valuable for use with low-cost sensors in collision prediction and avoidance applications.

I. INTRODUCTION

Vehicle trajectory estimation is a crucial part of selfdriving cars, collision warning systems, and traffic monitoring systems. Designing observers and estimation algorithms to estimate the trajectories of surrounding vehicles is valuable since such systems could be used to predict and prevent collisions. Exploiting such trajectory tracking systems is more critical when it comes to electric scooter users. On one hand, standing e-scooters have proliferated rapidly as an inexpensive and easily available mode of transportation. A market research company has predicted escooters will grow from a US\$14 billion global market in 2014 to \$37 billion in 2024 [1]. On the other hand, e-scooter riders are a vulnerable population on roads and are in significant danger of suffering from severe injuries in any carscooter collision [2]. The growth of e-scooter utilization and the vulnerability of the users are the two factors contributing to the increase in the number of injuries for e-scooter riders. As an example, a retrospective review was performed of the medical records of patients seen at an emergency department (ED) in Singapore [3], and there was found to be a 2.3-fold increase in the number of scooter-rider severe injuries from 2015 to 2016. It is shown in another study [4] that there were an estimated 70,644 ED visits for e-scooter-related injuries from 2014 to 2019 in the U.S. The estimated number of ED visits for e-scooter injuries increased from 8,269 visits in 2017 to 15,522 visits in 2018, showing the impact of the distribution of e-scooters in major cities by scooter-share companies in late 2017 [4].

By tracking the trajectories of nearby vehicles using lowcost sensors, a smart e-scooter can predict a potential collision and create a loud honk-like sound to alert the driver of the errant vehicle about the presence of the e-scooter.

II. RELATED WORK

A. Literature Review

The tracking of other vehicles on highways (and local roads) is typically done using radar, Lidar, cameras, or a combination of these sensors. Automotive radar provides reliable environmental perception in all-weather conditions at affordable cost but fails to supply semantic and geometry information due to the sparsity of radar detection points [5]. It is, however, an appropriate sensor for use in adaptive cruise control. In the case of e-scooters, radar may not be able to track all the vehicles at an upcoming intersection due to its limited field of view.

Detecting and tracking vehicle objects using 3D high-density Lidar is an approach that is viable for and often utilized on autonomous vehicles [6]. For example, the three-dimensional position and orientation (pose) is estimated in [6] using L-shaped fits to Lidar cloud data and then particle-filtering is utilized for vehicle trajectory tracking. High-density 3D Lidar sensors are, however, quite expensive and inappropriate for use on e-scooters.

Cameras are highly useful for lane marker detection, lateral lane offset computation, and many other object detection applications on advanced vehicles. A significant number of research publications consider the use of cameras and computer vision for detection and localization applications. For example, [7] proposes a framework that uses four visual sensors for a full surround view of a vehicle in order to achieve an understanding of surrounding vehicle behaviors. The trajectories are transformed to a common ground plane, where they are associated between perspectives and analyzed to reveal tendencies around the ego vehicle. Sensor fusion using a combination of millimeter-wave radar and cameras for object detection has also been pursued, as described in [8]. Further, the use of combined radar and camera for pedestrian detection and for occlusion-aware sensor fusion has been studied [9]. Maneuver classification and motion prediction of surrounding vehicles during complex traffic scenarios using vehicle-mounted multi-view cameras has also been pursued [10].

R. Rajamani and H. Alai are with the Department of Mechanical Engineering, University of Minnesota, Twin Cities, Minneapolis, MN 55455 USA (Email: rajamani@umn.edu; TEL: 612-626-7961; alai0003@umn.edu)

^{*} Research supported in part by a research grant from the National Science Foundation (NSF Grant CPS 2038403).

Another avenue of research has been the use of predicted trajectories for threat assessment. For example, [11] presents the use of Monte Carlo simulations to find threats in a road scene with the dynamic model used for the targets being similar to the one utilized in this present manuscript. An intelligent driver model has been utilized to analyze trajectory data from several German freeways showing different kinds of congested traffic forming near road inhomogeneities, specifically lane closings, intersections, or uphill gradients [12]. Likewise, a multiple model—based adaptive estimator (MMAE) that infers the lane-change intention of the surrounding vehicles and then predicts their trajectories has been studied in [13].

When it comes to vehicle tracking on an e-scooter platform, there are multiple challenges to designing such a collisionwarning system. Unlike autonomous vehicles that could be equipped with large and expensive sensors or processors, it is only reasonable to equip e-scooters with small and costeffective sensors. One possible option is low-density 2-D LIDAR sensors which are small, affordable, and can detect surrounding objects including vehicles. The problem with these low-cost sensors is that the reflection point from a target vehicle keeps changing due to the low density of measurements and hence there are many jumps/ discontinuities in the sensor data. Such uncertainties in measurement data make the observer design process challenging, specifically because vehicle motion models typically include nonlinear dynamics. Some previous studies addressed the problem of nonlinearity by turning the original model into multiple linear models and utilizing Interacting Multiple Model (IMM) filters (e. g. IMM Kalman Filters) for state estimation [14, 15]. These studies lack proof of stability, cannot cover all possible maneuvers, and are computationally demanding.

In our previous work [2], we implemented a linear matrix inequality (LMI) based nonlinear observer for vehicle tracking on an e-scooter. While the nonlinear observer has proof of stability and could estimate the vehicle's position and orientation in the presence of measurement uncertainties, its design requires assuming the velocity to be constant [16]. To overcome this issue, a coordinate transformation was found in [17] to allow for variable velocity and transformed the vehicle dynamics model into companion form. This transformation to companion form enabled the design of a stable high-gain observer with guaranteed feasibility. The high-gain observer [17] can estimate the position, velocity, orientation, and acceleration of the vehicles using a single high-gain matrix. However, with all the advantages of the high-gain observer, noise rejection is not addressed in its formulation. This causes unreliable estimates of velocity and orientation especially when using low-cost LIDAR sensors, with jumpy/noisy data.

B. Contributions

In contrast to the observers in literature where only the current measurement is used as part of their observer dynamics, here we use the last two consecutive measurements for estimation. Two consecutive measurements reveal important information about the displacement and direction

of movement of the vehicle, which enables us to have a multistage estimation for vehicle trajectories. Fig. 1 shows two consecutive measurement points from the location of a vehicle at two different time frames $(t_i \text{ and } t_{i-1})$. As can be seen, the vehicle direction of movement and its displacement are shown as α_i and S_i . We use these two new measurements in addition to the raw distance measurement of the vehicle to design three observers for speed, orientation, and position estimation. It is also shown that the three observers are robustly stable; the norm of the estimation errors will be bounded in the presence of uncertainties. The location measurement errors of the vehicles given by the sensors are assumed to be bounded (the boundaries are depicted as circles with radii d in Fig. 1). Therefore, it is assumed that the error of the resulting displacement and direction measurements α_i and S_i are bounded as well. A preliminary version of this paper is going to be presented at a conference [18]. However, detailed proofs could not be included and only two figures (one simulation and one experimental result) could be included in the conference paper. The major contributions of this paper are:

- The development of a multi-stage observer with guaranteed analytical stability proofs, allowing for variations in target vehicle velocity while also minimizing the influence of sensor noise on estimates.
- The implementation of the developed observer on an escooter platform using a low-cost 2D Lidar sensor and presentation of extensive experimental results.

The outline of the paper is as follows. Section III introduces the speed, orientation, and position models derived from the original vehicle kinematics equations. For each model, an observer is designed in section IV, and it is shown that the designed observers are guaranteed to have robust stability. Section V shows how these observers outperform a previous nonlinear observer [2] and a high-gain observer [8] in simulation and experiments respectively. Section VI contains the conclusions.

III. VEHICLE TRACKING MODEL

In this section, speed, orientation, and position models are obtained from the original vehicle kinematics. These models will be later used in section IV to design stable observers to track vehicle trajectories.

A. Original Bicycle- Model of Vehicle

Fig. 2 shows a vehicle with velocity V, orientation (yaw) angle ψ , slip angle β , and front steering angle δ_F . The vehicle (bicycle) equations are [19]:

$$\dot{X} = V\cos(\psi + \beta) \tag{1}$$

$$\dot{Y} = V \sin(\psi + \beta) \tag{2}$$

$$\dot{\psi} = V(\cos\beta) \tan\delta_F / l \tag{3}$$

where parameter l is the wheelbase length of the vehicle:

$$l = l_f + l_r \tag{4}$$

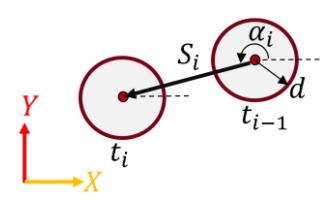


Fig. 1. Two consecutive measurements from the location of the vehicle at time frames t_i and t_{i-1} . The uncertainty boundary of the measurements is depicted as circles with radii d.

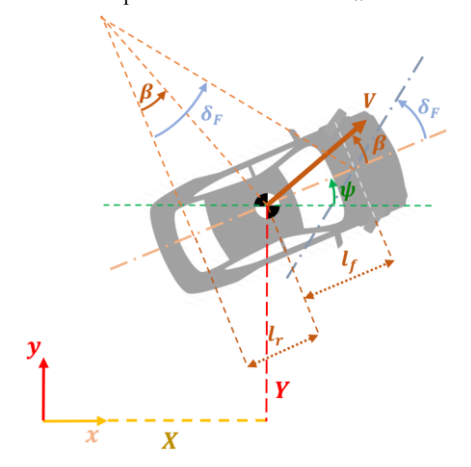


Fig. 2. Motion schematic and model variables for a Vehicle

Parameters l_f and l_r are shown in Fig. 2. The following relationship exists between the slip and steering angles [9]:

$$\beta = \tan^{-1} \left(\frac{l_r \tan(\delta_F)}{l_f + l_r} \right) \tag{5}$$

We are assuming that the non-ego vehicles only steer with their front wheels. Furthermore, it is assumed that the rate of steering angle and jerk are negligible:

$$\dot{\delta}_{\rm F} \approx 0 \tag{6}$$

$$\dot{I} \approx 0$$
 (7)

where $J = \ddot{V}$ represents the jerk of the vehicle or the derivative of the vehicle's acceleration.

In previous papers on the nonlinear observer and high gain observer ([2] and [8]), the non-ego vehicles were assumed to have constant velocities and accelerations respectively. Considering the constant jerk assumption in this paper, the performance of the observers designed here will be theoretically better than the previous ones in scenarios where the speed and acceleration are variable. The slip angle is assumed to lie within the following range:

$$-20^{\circ} \le \beta \le 20^{\circ} \tag{8}$$

For a typical vehicle with $l_r/l = 0.5$, the range for the front steering angle (based on (5) and (8)) will be:

$$-36^{\circ} \le \delta_F \le 36^{\circ} \tag{9}$$

which is better than what is assumed in [2]. In [2], the range of steering angles was assumed to be $-10^{\circ} \leq \delta_F \leq 10^{\circ}$, with the corresponding range of β being $-6^{\circ} \leq \beta \leq 6^{\circ}$. Note that assumptions (8) and (9) will be valid for typical vehicle motions and will only be violated under high-slip scenarios, for example when the vehicle is skidding on ice. Finally, it is assumed that:

$$l_r = 2 meters$$
 (10)

B. Linear Speed Model

As mentioned in section II, by using two consecutive measurements, we gain access to the displacement of the vehicles denoted as S_i in Fig. 1. Therefore, one can use displacement as the measurement in the speed model. By taking derivatives of the vehicle's displacement with respect to time, the speed model is derived. Consider the following state and output vectors:

$$s = [S \quad V \quad A \quad J]^T, \qquad y_s = S + d_s \tag{11}$$

where S and A represent the displacement and acceleration of the vehicle. Also, d_S represents the uncertainty related to displacement measurement. Based on (7):

$$\dot{s} = \begin{bmatrix} \dot{S} \\ \dot{V} \\ \dot{A} \\ \dot{I} \end{bmatrix} = \begin{bmatrix} V \\ A \\ J \\ 0 \end{bmatrix} = F_s s \tag{12}$$

and

$$y_s = H_s s + d_s \tag{13}$$

where:

$$F_s = \begin{bmatrix} 0 & 1 & 0 & 0 \\ 0 & 0 & 1 & 0 \\ 0 & 0 & 0 & 1 \\ 0 & 0 & 0 & 0 \end{bmatrix}, \qquad H_s = \begin{bmatrix} 1 & 0 & 0 & 0 \end{bmatrix} \quad (14)$$

As can be seen, the speed model derived here is linear.

C. Nonlinear Orientation Model

As mentioned in section II, by using two consecutive measurements, we gain access to the direction of motion of the vehicles denoted as α_i in Fig. 1. Equations (1) and (2) show that the direction of motion of a vehicle could be described as:

$$\alpha = \psi + \beta \tag{15}$$

Note that from (5) and (6) we have:

$$\dot{\beta} \approx 0 \tag{16}$$

Take the following state and output vectors:

$$z = [\psi \quad \beta]^T, \qquad y_z = \alpha + d_z \tag{17}$$

where d_z is the uncertainty of the angle measurement. Now taking derivative of (17) and using (3) and (16):

$$\dot{z} = \begin{bmatrix} \dot{\psi} \\ \dot{\beta} \end{bmatrix} = \begin{bmatrix} V(\cos\beta) \tan \delta_F / l \\ 0 \end{bmatrix}$$
 (18)

Replace (5) in (18):

$$\dot{z} = \begin{bmatrix} \dot{\psi} \\ \dot{\beta} \end{bmatrix} = \begin{bmatrix} V \sin \beta / l_r \\ 0 \end{bmatrix} = \begin{bmatrix} u_z f(z) / l_r \\ 0 \end{bmatrix}$$
 (19)

and

$$y_z = H_z z + d_z, \qquad u_z = V \tag{20}$$

where u_z is the input to this system and:

$$f(z) = \sin \beta$$
, $H_z = [1 \ 1]$ (21)

The orientation model derived here is nonlinear. Note that our knowledge about the input of this system (speed) is indirect and will depend on the performance of the speed observer. We will use the estimated speed when designing the orientation observer, instead of the actual speed but will account for the error of the speed estimation.

D. Linear Position Model

Consider the following state and output vectors:

$$w = [x \quad y]^T, \qquad y_w = w + d_w \tag{22}$$

Taking derivative of the state vector using (1) and (2):

$$\dot{w} = \begin{bmatrix} \dot{x} \\ \dot{y} \end{bmatrix} = \begin{bmatrix} V \cos(\psi + \beta) \\ V \sin(\psi + \beta) \end{bmatrix} = g(u_w)$$
 (23)

where u_w is the input to this system. Note that our knowledge about the inputs of this system (speed and orientation) is limited and will depend on the performance of the speed and orientation observers. We will use the estimated speed and orientation instead of their actual values when designing the position observer but will account for the errors in these estimations.

IV. MULTI-STAGE OBSERVER DESIGN

In this section, we design stable observers based on the models introduced in section III. Take \hat{w} , \hat{V} , \hat{A} , $\hat{\psi}$, and $\hat{\beta}$ as the estimates of vehicle location, speed, orientation, and slip angle. The estimated error variables are defined as $\widetilde{w} = w \widehat{w}$, $\widetilde{V} = V - \widehat{V}$, $\widetilde{A} = A - \widehat{A}$, $\widetilde{\psi} = \psi - \widehat{\psi}$, and $\widetilde{\beta} = \beta - \widehat{\beta}$. The structure of the estimation algorithm is described in Fig. 3. The speed observer limits the second norm of the estimated speed error. The orientation observer limits the second norm of the estimated orientation angle error, and the position observer limits the second norm of the estimated location

A. Speed Observer Design

The goal here is to design a robust observer for the model (12)- (14). Assuming that the measurement uncertainties are bounded, the goal is to guarantee bounded error for the states:

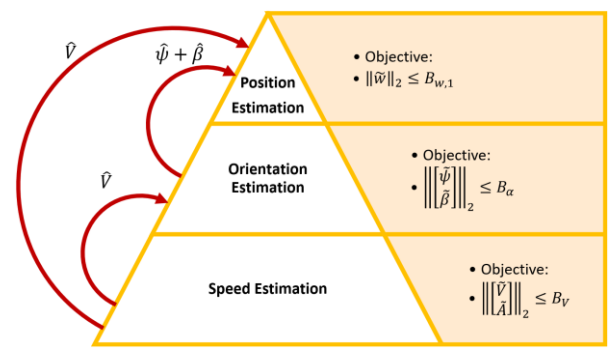


Fig. 3. Schematic of the trajectory estimation algorithm.

Goal:
$$\| \begin{bmatrix} \tilde{V} \\ \tilde{A} \end{bmatrix} \|_2 \le B_V$$
, Assumption: $\| d_s \|_2 \le B_s$ (24)

The goal in equation (24) can be identically transformed to the one in equation (25) using the transformation $\begin{vmatrix} V \\ \tilde{\Lambda} \end{vmatrix} = q_V \tilde{s}$.

$$\|q_V \tilde{s}\|_2 \le \sqrt{\mu_s} \|d_s\|_2, \text{ with } q_V = \begin{bmatrix} 0 & 0 & 0 & 0 \\ 0 & 1 & 0 & 0 \\ 0 & 0 & 1 & 0 \\ 0 & 0 & 0 & 0 \end{bmatrix}$$
 (25)

where
$$\tilde{s} = s - \hat{s}$$
, and $\sqrt{\mu_s} = B_V/B_s$. Rewrite (25) as:

$$Goal: \tilde{s}^T q_V^T q_V \tilde{s} \le \mu_s d_s^T d_s \tag{26}$$

The observer dynamics are defined to be:

$$\dot{\hat{\mathbf{s}}} = F_{\mathbf{s}}\hat{\mathbf{s}} + L_{\mathbf{s}}(y_{\mathbf{s}} - H_{\mathbf{s}}\hat{\mathbf{s}}) \tag{27}$$

where L_s is the constant speed observer gain matrix. The observer error dynamics \tilde{s} is derived by subtracting (27) from (12) and replacing (13):

$$\dot{\tilde{s}} = \dot{s} - \dot{\hat{s}} = F_s s - F_s \hat{s} - L_s (y_s - H_s \hat{s}) = (F_s - L_s H_s) \tilde{s} - L_s d_s$$
 (28)

where $\tilde{s} = s - \hat{s}$.

Theorem 1. If there exists a Hermitian matrix $P_s > 0$, an

observer gain matrix
$$L_s$$
 and a positive scalar ϵ_s such that:
$$\begin{bmatrix} (F_s - L_s H_s)^T P_s + P_s (F_s - L_s H_s) + \epsilon_s q_V^T q_V & -P_s L_s \\ -L_s^T P_s & -\epsilon_s \mu_s \end{bmatrix} < 0 \quad (29)$$

then, the goal (26) will be achieved.

Proof. First assume that the goal (26) is not yet achieved:

$$\tilde{s}^T q_V^T q_V \tilde{s} > \mu_s d_s^T d_s \tag{30}$$

Writing (30) in matrix form:

$$V_1 = \begin{bmatrix} \tilde{s} \\ d_s \end{bmatrix}^T \begin{bmatrix} -q_V^T q_V & 0 \\ 0 & \mu_s \end{bmatrix} \begin{bmatrix} \tilde{s} \\ d_s \end{bmatrix} < 0$$
 (31)

Consider the following Lyapunov function candidate:

$$V_{Lyp,s} = \tilde{s}^T P_s \tilde{s}, \qquad P_s > 0 \tag{32}$$

where P_s is Hermitian. Taking derivative of this Lyapunov function:

$$\dot{V}_{Lyns} = \dot{\tilde{s}}^T P_s \tilde{s} + \tilde{s}^T P_s \dot{\tilde{s}} \tag{33}$$

Replace (28) in (33):

$$\dot{V}_{Lyp,s} = \tilde{s}^{T} [(F_{s} - L_{s}H_{s})^{T}P_{s} + P_{s}(F_{s} - L_{s}H_{s})]\tilde{s} - d_{s}^{T}L_{s}^{T}P_{s}\tilde{s} - \tilde{s}^{T}P_{s}L_{s}d_{s}$$
(34)

Writing (34) in matrix form:

$$\dot{V}_{Lyp,s} = \begin{bmatrix} \tilde{s} \\ d_s \end{bmatrix}^T \begin{bmatrix} (F_s - L_s H_s)^T P_s + P_s (F_s - L_s H_s) & -P_s L_s \\ -L_s^T P_s & 0 \end{bmatrix} \begin{bmatrix} \tilde{s} \\ d_s \end{bmatrix} \tag{35}$$

If the derivative of Lyapunov function is negative definite or $\dot{V}_{Lyp,s} < 0$, the goal (26) will be achieved. Using the S-procedure lemma [20], $\dot{V}_{Lyp,s} < 0$ if and only if there exists a positive scalar $\epsilon_s > 0$ such that:

$$\dot{V}_{Lyp,s} < \epsilon_s V_1$$

Substituting from (31) and (35), it follows that a sufficient condition for stability is:

$$\begin{bmatrix} (F_s - L_s H_s)^T P_s + P_s (F_s - L_s H_s) & -P_s L_s \\ -L_s^T P_s & 0 \end{bmatrix} < \epsilon_s \begin{bmatrix} -q_V^T q_V & 0 \\ 0 & \mu_s \end{bmatrix}$$

This is nothing but the LMI (29) and the proof is therefore complete.

Remarks on LMIs: Inequality (29) is equivalent to a linear matrix inequality (LMI). LMIs are inequalities that are linear in the matrix variables whose values need to be solved for. Excellent numerical tools exist for solving such LMIs [20], [21] including software tools that can be easily utilized in MATLAB [22]. While inequality (29) appears to have bilinear terms involving P_sL_s , this bilinear term can be replaced using the transformation $Y_s = P_sL_s$ [20]. Then the new form of (29) becomes

$$\begin{bmatrix} F_s^T P_s - H_s^T Y_s^T + P_s F_s - Y_s H_s + \varepsilon_s q_V^T q_V & -Y_s \\ -Y_s^T & -\varepsilon_s \mu_s \end{bmatrix} < 0$$
 (36)

This transformed inequality is clearly linear in the variables P_S and Y_S . The LMI Toolbox in MATLAB [22] can then be used for solving this LMI. Once $P_S > 0$ and Y_S are obtained, L_S can be obtained using $L_S = P_S^{-1}Y_S$.

For the assumed operating range of equations (8) and (9), the following observer gain solution satisfies LMI problem (29):

$$L_s = [4.61 \quad 12.24 \quad 9.83 \quad 4.16]^T$$

B. Orientation Observer Design

The goal here is to design a robust observer for the model (19)- (21). Assuming that the measurement uncertainties are bounded, the goal is to guarantee bounded error for the states:

Goal:
$$\left\| \begin{bmatrix} \tilde{\psi} \\ \tilde{\beta} \end{bmatrix} \right\|_{2} \le B_{\alpha},$$
 (37)

Assumption: $||d_z||_2 + ||\tilde{V}||_2 \le B_z$

Based on the assumption in (37), the goal is translated to:

$$\|q_{\alpha}\tilde{z}\|_{2} \le \sqrt{\mu_{z}} \left(\|d_{z}\|_{2} + \|\tilde{V}\|_{2}\right), \qquad q_{\alpha} = \begin{bmatrix} 1 & 0\\ 0 & 1 \end{bmatrix}$$
(38)

where z is defined in (17) and $\sqrt{\mu_z} = B_\alpha/B_z$. Rewrite (38) as:

Goal:
$$\tilde{z}^T q_\alpha \tilde{z} \le \mu_d d_z^T d_z + \mu_d \tilde{V}^T \tilde{V}$$
 (39)

Take the following observer dynamics:

$$\dot{\hat{z}} = \begin{bmatrix} \hat{V}f(\hat{z})/l_r \\ 0 \end{bmatrix} + L_z(y_z - H_z\hat{z})$$
 (40)

where L_z is the constant orientation observer gain matrix. The observer error dynamics \tilde{z} is derived by subtracting (40) from (19) and replacing (20):

$$\dot{\tilde{z}} = \dot{z} - \dot{\tilde{z}} = \begin{bmatrix} (Vf - \hat{V}\hat{f})/l_r \\ 0 \end{bmatrix} - L_z H_z \tilde{z} - L_z d_z \quad (41)$$

where $\tilde{z} = z - \hat{z}$ and $\hat{f} = f(\hat{z})$. Add and subtract $V\hat{f}/l_r$ to the first row of (41):

$$\dot{\tilde{z}} = \begin{bmatrix} (Vf - V\hat{f} + V\hat{f} - \hat{V}\hat{f})/l_r \\ 0 \end{bmatrix} - L_z H_z \tilde{z} - L_z d_z \ (42)$$

01

$$\dot{\tilde{z}} = G(V\tilde{f}/l_r) + G(\tilde{V}\hat{f}/l_r) - L_z H_z \tilde{z} - L_z d_z$$
 (43)

where $G = \begin{bmatrix} 1 & 0 \end{bmatrix}^T$ and $\tilde{f} = f - \hat{f}$.

Lemma 1. Considering (8) and (21), the following inequalities are valid for \tilde{f} :

and

$$V_{3} = \begin{bmatrix} \tilde{z} \\ \tilde{f} \\ \tilde{V}\hat{f}/l_{r} \\ d_{z} \end{bmatrix}^{T} \begin{bmatrix} q_{\beta}^{T}q_{\beta} & -\rho_{2}q_{\beta}^{T} & 0 & 0 \\ -\rho_{2}q_{\beta} & 1 & 0 & 0 \\ 0 & 0 & 0 & 0 \end{bmatrix} \begin{bmatrix} \tilde{z} \\ \tilde{f} \\ \tilde{V}\hat{f}/l_{r} \\ d_{z} \end{bmatrix} \ge 0 \quad (45)$$

where $q_{\beta} = [0 \ 1]$, and ρ_1 and ρ_2 are lower bounds on $\cos(\beta)$ and $\cos^2(\beta)$ as shown in equation (50).

Proof. Using the Mean Value Theorem (MVT) and (21):

$$\tilde{f}(\hat{z}, z) = \sin \beta - \sin \hat{\beta} = \cos \bar{\beta} \,\tilde{\beta} \tag{46}$$

where $\bar{\beta}$ is some value between β and $\hat{\beta}$. Therefore:

$$\left(\tilde{f}(\hat{z},z) - \cos\bar{\beta}\,\tilde{\beta}\right)^2 = 0\tag{47}$$

or

$$\tilde{f}^T \tilde{f} + (\cos^2 \bar{\beta}) \tilde{\beta}^T \tilde{\beta} - \cos \bar{\beta} (\tilde{f}^T \tilde{\beta} + \tilde{\beta}^T \tilde{f}) = 0 \quad (48)$$

Note that for $-20^{\circ} \le \beta \le 20^{\circ}$, the function $\sin \beta$ is monotonically increasing. Therefore:

$$\tilde{f}^T \tilde{\beta} = \tilde{\beta}^T \tilde{f} \ge 0 \tag{49}$$

Also, for the given range:

$$0.94 = \rho_2 \le \cos \bar{\beta} \le 1, 0.88 = \rho_1 \le \cos^2 \bar{\beta} \le 1$$
 (50)

Using (49) and (50):

$$\tilde{f}^{T}\tilde{f} + \rho_{1}\tilde{\beta}^{T}\tilde{\beta} - (\tilde{f}^{T}\tilde{\beta} + \tilde{\beta}^{T}\tilde{f})$$

$$\leq \tilde{f}^{T}\tilde{f} + \cos^{2}\tilde{\beta}\tilde{\beta}^{T}\tilde{\beta} - \cos\tilde{\beta}(\tilde{f}^{T}\tilde{\beta} + \tilde{\beta}^{T}\tilde{f})$$

$$\leq \tilde{f}^{T}\tilde{f} + \tilde{\beta}^{T}\tilde{\beta} - \rho_{2}(\tilde{f}^{T}\tilde{\beta} + \tilde{\beta}^{T}\tilde{f})$$
(51)

Now replace $\tilde{\beta} = q_{\beta}\tilde{z}$ and (48) in (51):

$$\tilde{f}^T \tilde{f} + \rho_1 \tilde{z}^T q_\beta^T q_\beta \tilde{z} - (\tilde{f}^T q_\beta \tilde{z} + \tilde{z}^T q_\beta^T \tilde{f}) \leq 0
\leq \tilde{f}^T \tilde{f} + \tilde{z}^T q_\beta^T q_\beta \tilde{z} - \rho_2 (\tilde{f}^T q_\beta \tilde{z} + \tilde{z}^T q_\beta^T \tilde{f})$$
(52)

Rewriting these two inequalities in matrix form, we will have (44) and (45).

Lemma 2. If the following inequality is satisfied, goal (39) is also satisfied:

$$V_{4} = \begin{bmatrix} \tilde{z} \\ \tilde{f} \\ \tilde{V}\hat{f}/l_{r} \\ d_{z} \end{bmatrix}^{T} \begin{bmatrix} -q_{\alpha} & 0 & 0 & 0 \\ 0 & 0 & 0 & 0 \\ 0 & 0 & \mu_{V} & 0 \\ 0 & 0 & 0 & \mu_{d} \end{bmatrix} \begin{bmatrix} \tilde{z} \\ \tilde{f} \\ \tilde{V}\hat{f}/l_{r} \\ d_{z} \end{bmatrix} \ge 0 \quad (53)$$

where:

$$\mu_V = 36 \times \mu_d \tag{54}$$

Proof. First, note that from (8) and (10):

$$(\hat{f}/l_r)^T (\hat{f}/l_r) = \sin^2 \hat{\beta} / l_r^2 \le 1/36$$
 (55)

Therefore:

$$\begin{bmatrix} \tilde{z} \\ \tilde{f} \\ \tilde{V}\hat{f}/l_r \end{bmatrix}^T \begin{bmatrix} -q_{\alpha} & 0 & 0 & 0 \\ 0 & 0 & 0 & 0 \\ 0 & 0 & \mu_V & 0 \\ 0 & 0 & 0 & \mu_d \end{bmatrix} \begin{bmatrix} \tilde{z} \\ \tilde{f} \\ \tilde{V}\hat{f}/l_r \end{bmatrix}$$

$$\leq \mu_V \tilde{V}^T \tilde{V}/36 + \mu_d d_z^T d_z - \tilde{z}^T q_{\alpha} \tilde{z}$$
(56)

Replace (54) in (56) and use (53):

$$0 \leq \begin{bmatrix} \tilde{z} \\ \tilde{f} \\ \tilde{V}\hat{f}/l_r \end{bmatrix}^{l} \begin{bmatrix} -q_{\alpha} & 0 & 0 & 0 \\ 0 & 0 & 0 & 0 \\ 0 & 0 & \mu_{V} & 0 \\ 0 & 0 & 0 & \mu_{d} \end{bmatrix} \begin{bmatrix} \tilde{z} \\ \tilde{f} \\ \tilde{V}\hat{f}/l_r \\ d_z \end{bmatrix}$$
(57)
$$\leq \mu_{d} \tilde{V}^{T} \tilde{V} + \mu_{d} d_{z}^{T} d_{z} - \tilde{z}^{T} q_{\alpha} \tilde{z}$$

which is the goal (39) and the proof is complete.

Theorem 2. If there exists a Hermitian matrix $P_z > 0$, an observer gain matrix L_z and positive scalars $\epsilon_{z,1}$, $\epsilon_{z,2}$ and $\epsilon_{z,3}$ such that:

then, the goal (53) (or equivalently (39)) will be achieved. **Proof.** First assume that the goal (53) is not yet achieved:

$$\begin{bmatrix} \tilde{z} \\ \tilde{f} \\ \tilde{V}\hat{f}/l_r \\ d_z \end{bmatrix}^T \begin{bmatrix} -q_{\alpha} & 0 & 0 & 0 \\ 0 & 0 & 0 & 0 \\ 0 & 0 & \mu_V & 0 \\ 0 & 0 & 0 & \mu_d \end{bmatrix} \begin{bmatrix} \tilde{z} \\ \tilde{f} \\ \tilde{V}\hat{f}/l_r \\ d_z \end{bmatrix} \le 0$$
 (59)

Consider the following Lyapunov function candidate:

$$V_{Lyp,z} = \tilde{z}^T P_z \tilde{z}, \qquad P_z > 0 \tag{60}$$

where P_z is Hermitian. Taking derivative of this Lyapunov function:

$$\dot{V}_{LVD,Z} = \dot{\tilde{z}}^T P_Z \tilde{z} + \tilde{z}^T P_Z \dot{\tilde{z}} \tag{61}$$

Replace (43) in (61):

$$\dot{V}_{Lyp,z} = (G(V\tilde{f}/l_r) + G(\tilde{V}\hat{f}/l_r) - L_zH_z\tilde{z} - L_zd_z)^T P_z\tilde{z}
+ \tilde{z}^T P_z(G(V\tilde{f}/l_r) + G(\tilde{V}\hat{f}/l_r) - L_zH_z\tilde{z} - L_zd_z)$$
(62)

Writing (62) in matrix form:

$$V_{Lyp,z} = \begin{bmatrix} \tilde{z} \\ \tilde{f} \\ \tilde{V}\hat{f}/l_r \\ d_z \end{bmatrix}^T \begin{bmatrix} P_z L_z H_z - H_z^T L_z^T P_z & P_z G V/l & P_z G & -P_z L_z \\ G^T P_z V/l & 0 & 0 & 0 \\ G^T P_z & 0 & 0 & 0 \\ -L_r^T P_z & 0 & 0 & 0 \end{bmatrix} \begin{bmatrix} \tilde{z} \\ \tilde{f} \\ \tilde{V}\hat{f}/l_r \\ d_z \end{bmatrix}$$
(63)

If the derivative of the Lyapunov function candidate is negative definite or $\dot{V}_{Lyp,z} < 0$, the goal (39) will be eventually achieved. Using the S- procedure lemma [20], $\dot{V}_{Lynz} < 0$ if and only if:

$$\dot{V}_{LVDZ} < \epsilon_{Z1}V_2 - \epsilon_{Z2}V_3 + \epsilon_{Z3}V_4$$

 $\dot{V}_{Lyp,z} < \epsilon_{z,1}V_2 - \epsilon_{z,2}V_3 + \epsilon_{z,3}V_4$ where V_2 , V_3 and V_4 are defined in Lemma 1 and Lemma 2. Substituting for V_2 , V_3 and V_4 from equations (44), (45) and (53) and for $\dot{V}_{Lyp,z}$ from equation (63), the LMI (58) directly follows. The proof is thus complete.

The observer gains are obtained for various nominal speeds each representing a range of speed. The LMI (58) is solved for the minimum and maximum values in those spans. The observer gains are provided in Table 1:

TABLE I OBSERVER GAINS FOR VARIOUS NOMINAL SPEEDS

	Observer Gain for Various Nominal Speeds (m/s)								
V_{nom} :	1	1.5	2	3	4	5	6		
$L_z(1)$:	0.89	0.98	1.37	1.76	2.52	3.67	5.47		
$L_z(2)$:	0.25	0.27	0.30	0.33	0.37	0.50	0.70		
	Observer Gain for Various Nominal Speeds (m/s)								
V_{nom} :	7	8	9	10	11	12	13		
$L_z(1)$:	8.05	9.70	5.58	6.08	6.60	7.14	7.70		
$L_z(2)$:	0.99	1.17	0.66	0.68	0.71	0.74	0.77		
	Observer Gain for Various Nominal Speeds (m/s)								
V_{nom} :	14	15	16	17	18	19	20		
$L_z(1)$:	8.27	8.84	9.42	9.99	10.49	10.97	11.44		
$L_z(2)$:	0.79	0.82	0.85	0.88	0.89	0.91	0.92		

As an example, if the output of the speed observer is $\hat{V} = 6.7 \, m/s$, then the observer gain $L_z = [8.05 \, 0.99]^T$ should be used for angle estimation. In other words, the value of the nominal speed is at the midpoint of the speed range for each entry in the table. The gains in the table can be directly used and no interpolation is needed.

C. Position Observer Design

The goal here is to design a robust observer for the model (22)- (23). Take the following observer dynamics:

$$\dot{\widehat{w}} = g(\widehat{w}) + L_w(y_w - \widehat{w}) \tag{64}$$

where $g(\widehat{w}) = [\widehat{V}\cos(\widehat{\psi} + \widehat{\beta}) \quad \widehat{V}\sin(\widehat{\psi} + \widehat{\beta})]^T$ and L_w is the constant position observer gain matrix. The observer error dynamics \widetilde{w} is derived by subtracting (64) from (23):

$$\dot{\widetilde{w}} = \dot{w} - \dot{\widehat{w}} = \widetilde{g}(w, \widehat{w}) - L_w \widetilde{w} - L_w d_w$$

$$= \begin{bmatrix} V \cos(\psi + \beta) - \widehat{V} \cos(\widehat{\psi} + \widehat{\beta}) \\ V \sin(\psi + \beta) - \widehat{V} \sin(\widehat{\psi} + \widehat{\beta}) \end{bmatrix} - L_w \widetilde{w} - L_w d_w$$
(65)

where $\widetilde{w} = w - \widehat{w}$ and $\widetilde{g}(w, \widehat{w}) = g(w) - g(\widehat{w})$. Assuming that the measurement uncertainties are bounded, goal is to guarantee bounded error for the states:

$$Goal: \|\widetilde{w}\|_{2} \le B_{w,1},$$
 Assumption: $\|d_{w}\|_{2} + \|\widetilde{g}\|_{2} \le B_{w,2}$ (66)

Note that:

$$\|\tilde{g}\|_{2} = \sqrt{V^{2} + \hat{V}^{2} - 2V\hat{V}\cos(\tilde{\psi} + \tilde{\beta})}$$

$$\leq \sqrt{\tilde{V}^{2} + 2V\hat{V}(\tilde{\psi} + \tilde{\beta})^{2}}$$
(67)

Therefore, it is reasonable to assume that $\|\tilde{g}\|_2$ is bounded in (66) $(\tilde{V}, \tilde{\psi}, \text{ and } \tilde{\beta} \text{ are all bounded because of the orientation and speed observers).$

Based on assumption in (66), the goal is translated to:

$$\|\widetilde{w}\|_{2} \le \sqrt{\mu_{w}}(\|d_{w}\|_{2} + \|\widetilde{g}\|_{2})$$
 (68)

where $\sqrt{\mu_w} = B_{w,1}/B_{w,2}$. Rewrite (68) as:

Goal:
$$\widetilde{w}^T \widetilde{w} \le \mu_w d_w^T d_w + \mu_w \widetilde{g}^T \widetilde{g}$$
 (69)

Theorem 3. If there exists Hermitian $P_w > 0$ and L_w such that:

$$\begin{bmatrix} -L_w^T P_w - P_w L_w & P_w & -P_w L_w \\ P_w & 0 & 0 \\ -L_w^T P_w & 0 & 0 \end{bmatrix} < \varepsilon_w \begin{bmatrix} -I & 0 & 0 \\ 0 & \mu_w & 0 \\ 0 & 0 & \mu_w \end{bmatrix} (70)$$

then, the goal (69) will be achieved.

Proof. First assume that the goal (69) is not yet achieved:

$$\widetilde{w}^T \widetilde{w} \ge \mu_w d_w^T d_w + \mu_w \widetilde{g}^T \widetilde{g} \tag{71}$$

Then writing (71) in matrix form:

$$V_{5} = \begin{bmatrix} \widetilde{w} \\ \widetilde{g} \\ d_{w} \end{bmatrix}^{T} \begin{bmatrix} -I & 0 & 0 \\ 0 & \mu_{w} & 0 \\ 0 & 0 & \mu_{w} \end{bmatrix} \begin{bmatrix} \widetilde{w} \\ \widetilde{g} \\ d_{w} \end{bmatrix} \le 0$$
 (72)

Consider the following Lyapunov function candidate:

$$V_{Lyp,w} = \widetilde{w}^T P_w \widetilde{w}, \qquad P_w > 0 \tag{73}$$

and P_w is Hermitian. Taking derivative of this Lyapunov function:

$$\dot{V}_{Lvp,w} = \dot{\widetilde{w}}^T P_w \widetilde{w} + \widetilde{w}^T P_w \dot{\widetilde{w}} \tag{74}$$

Replace (65) in (74):

$$\dot{V}_{Lyp,w} = \tilde{g}^T P_w \widetilde{w} - \widetilde{w}^T L_w^T P_w \widetilde{w} - d^T L_w^T P_w \widetilde{w} + \widetilde{w}^T P_w \widetilde{g} - \widetilde{w}^T P_w L_w \widetilde{w} - \widetilde{w}^T P_w L_w d_w$$
(75)

Writing (75) in matrix form:

$$\dot{V}_{Lyp,w} = \begin{bmatrix} \widetilde{w} \\ \widetilde{g} \\ d_w \end{bmatrix}^T \begin{bmatrix} -L_w^T P_w - P_w L_w & P_w & -P_w L_w \\ P_w & 0 & 0 \\ -L_w^T P_w & 0 & 0 \end{bmatrix} \begin{bmatrix} \widetilde{w} \\ \widetilde{g} \\ d_w \end{bmatrix}$$
(76)

If the derivative of the Lyapunov function is negative definite or $\dot{V}_{Lyp,w} < 0$, the goal (69) will be eventually achieved. Using the S- procedure lemma, $\dot{V}_{Lyp,w} < 0$ if and only if

$$\dot{V}_{L\nu p.w} < \epsilon_w V_5$$

Substituting for $\dot{V}_{Lyp,w}$ from equation (76) and for V_5 from equation (72), the inequality specified in (70) (i.e., in the statement of the Theorem) directly follows. The proof is therefore complete.

For the assumed operating range of equations (8) and (9), the observer gain solution L_w obtained by solving the LMI problem (70) is found to be:

$$L_w = \begin{bmatrix} 20 & 0\\ 0 & 20 \end{bmatrix} \tag{77}$$

V. SIMULATIONS AND EXPERIMENTS

A. Simulation Results

In this section, the multi-stage observer is compared to previously designed nonlinear [2] and high-gain observers [17] in simulation. As shown in Fig. 4, all the observers have a good performance when the speed and vehicle orientation are constant, one of the simple scenarios that could occur. Fig. 5 shows all the observers having acceptable performance when the speed is constant, but the orientation angle is changing. The high-gain observer is the best, and the multistage observer outperforms the nonlinear LMI observer in orientation estimation.

The nonlinear observer in [2] was designed based on a constant velocity assumption (using $V = 10 \, m/s$) due to limitations in exploiting the Mean Value Theorem (MVT) [16]. Therefore, the multi-stage observer and the high-gain observer both outperform the nonlinear observer in scenarios where the speed is not constant. This is visible in Fig. 6, where the scenario includes variable speed.

As can be seen in Fig. 5 and Fig. 6, the convergence rate of the multi-stage observer is slower than the high-gain observer, as the gains of the multi-stage observer are smaller because of the H_{∞} constraint exploited in the LMI problems. While this feature slows down the convergence rate, it is necessary for noise rejection. The estimation results of the multi-stage observer are smoother than the high-gain observer in realworld scenarios as the noise rejection constraint is not included in the high-gain observer design [17].

Using previous data to approximately measure speed and orientation as measurements can cause additional errors in the multi-stage observer. The effects of these approximations are visible as small offset errors in the simulations of the multistage observer. We accept this disadvantage to be able to improve the results compared to the nonlinear observer in terms of relaxing the constant velocity assumption, and the high gain observer in terms of noise rejection. Except for the minor disadvantages of the multi-stage observer over the high-gain observer, both show promising results in theory and simulation. In the experimental results, however, the multistage observer outperforms the high-gain observer in speed and orientation estimation. In the experimental results, we also present additional comparisons with an extended Kalman filter which is a standard nonlinear estimation algorithm for systems with noise.

The root-mean-square errors of the observers for the simulation results are presented in Table 2. The results show that the high-gain observer has the best performance since there is no added noise in the simulations. It will be shown in experimental results that the multi-stage observer works better in terms of noise rejection. The nonlinear observer performs poorly compared to the other two observers in cases where the speed is variable.

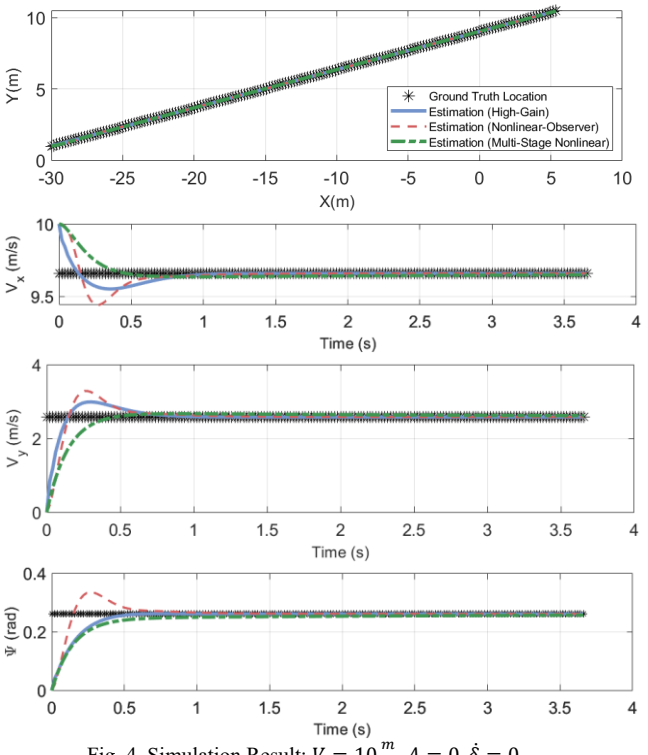


Fig. 4. Simulation Result: $V = 10 \frac{m}{s}$, A = 0, $\dot{\delta} = 0$

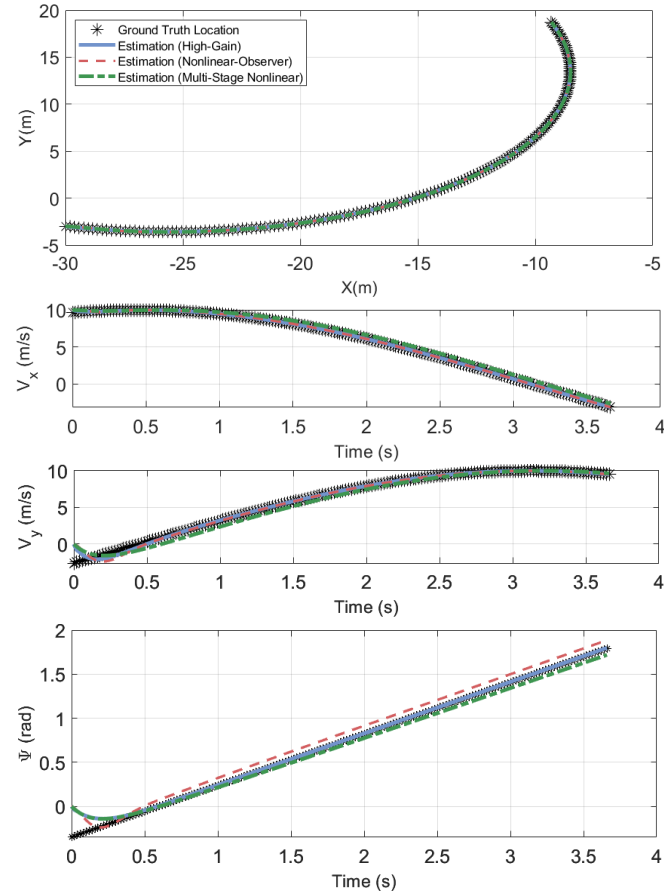


Fig. 5. Simulation Result: $V = 10 \frac{m}{s}$, A = 0, $\dot{\delta} = 10 \frac{deg}{s}$

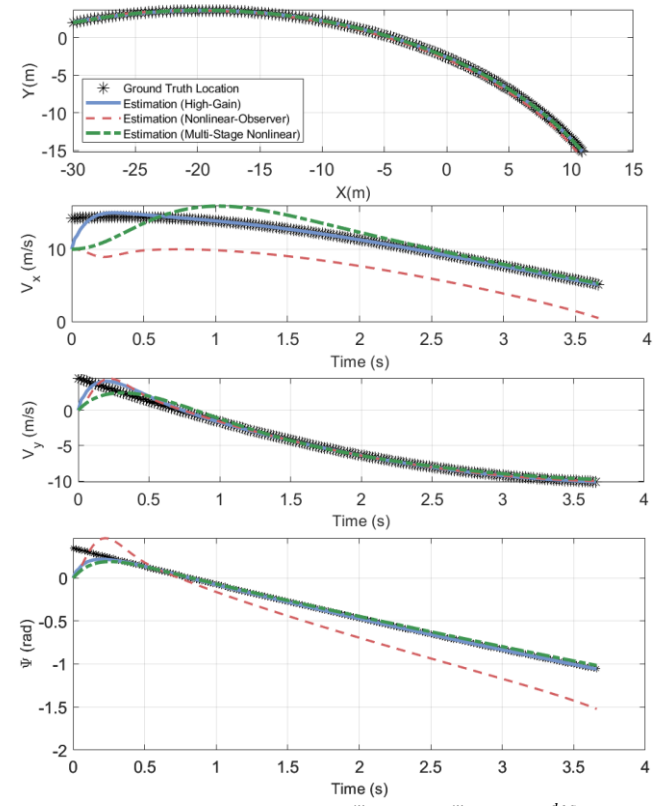


Fig. 6. Simulation Result: $V = 15 \frac{m}{s}$, $A = -1 \frac{m}{s^2}$, $\dot{\delta} = -5 \frac{deg}{s}$

TABLE II
OBSERVERS' RMSE VALUES IN SIMULATIONS

OBSERVERS RIVISE VALUES IN SINICEATIONS										
Case #	Observer Type	<i>w</i> (m)	\widetilde{V}_x (m/s)	$\widetilde{V_y}$ (m/s)	$ ilde{\psi}$ (rad)					
Simulation 1:	Nonlinear	0.01	0.07	0.38	0.04					
A = 0	High-Gain	0.00	0.05	0.29	0.04					
$\dot{\delta} = 0$	Multi-Stage	0.01	0.07	0.38	0.04					
Simulation 2:	Nonlinear	0.01	0.07	0.4	0.10					
A = 0	High-Gain	0.00	0.06	0.3	0.05					
$\dot{\delta} = 10^{\circ}/s$	Multi-Stage	0.01	0.40	0.6	0.07					
Simulation 3:	Nonlinear	0.27	4.09	0.68	0.25					
$A = -1 m/s^2$	High-Gain	0.00	0.48	0.55	0.04					
$\dot{\delta} = -5^{\circ}/s$	Multi-Stage	0.04	1.64	0.74	0.06					

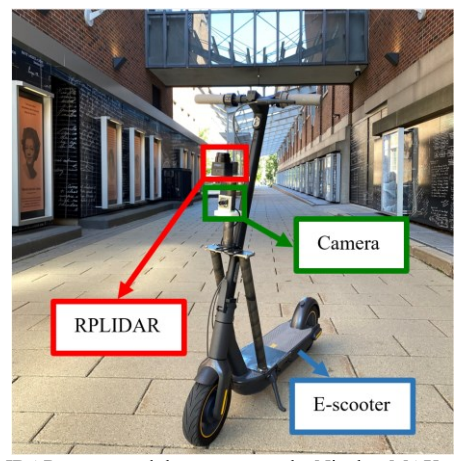


Fig. 7. RPLIDAR sensor and the camera on the Ninebot MAX e-Scooter.

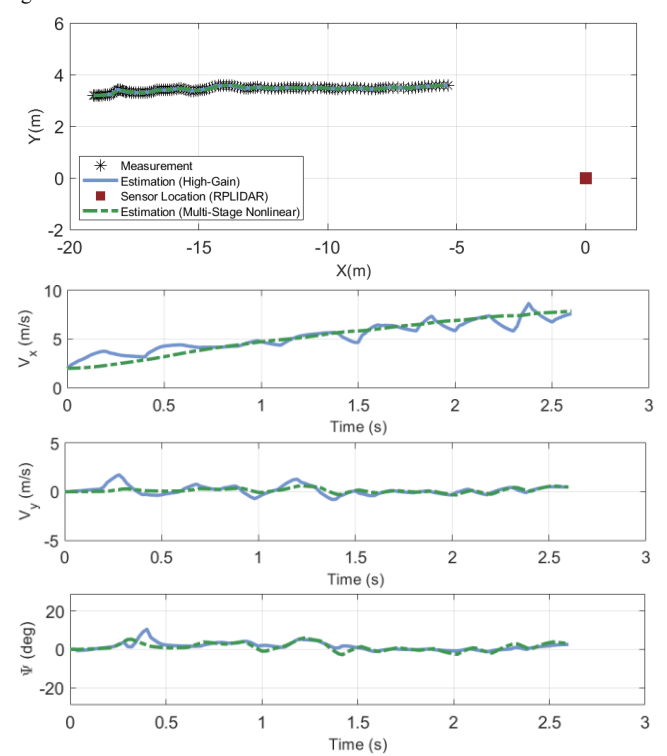


Fig. 8. Experimental Results of Scenario 1 in which the vehicle moves straight from left to right perpendicular to the e-scooter's direction. The high-gain and the multi-stage nonlinear observers are compared.

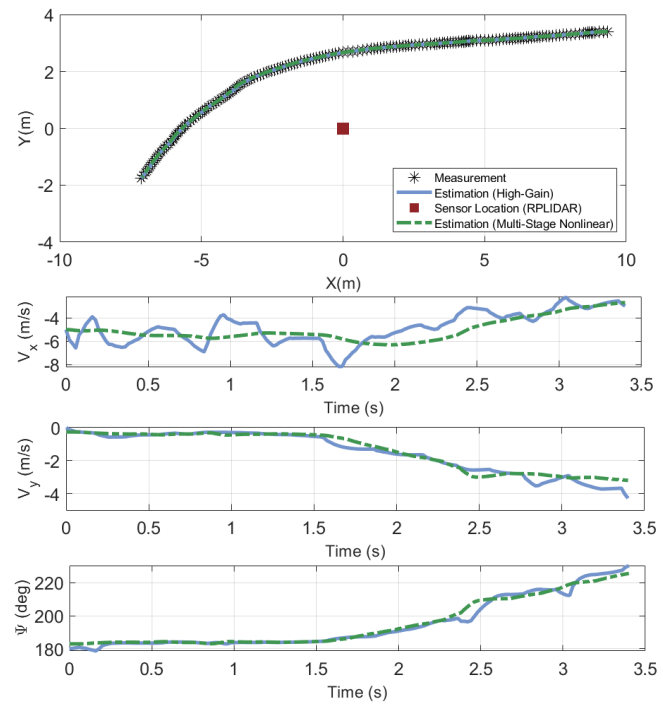


Fig. 9. Experimental Results of Scenario 2 in which the vehicle turns left in front of the e-scooter and eventually travels opposite to the e-scooter's direction. The high-gain and multi-stage nonlinear observers are compared.

B. Experimental Results

Fig. 7 shows our experimental setup including a RPLIDAR Mapper sensor mounted on a Ninebot MAX e-scooter. The RPLIDAR is an affordable sensor that provides a low-density 2-D point cloud map of the environment. The RPLIDAR's reflection points from moving objects in the environment (here vehicles) keep changing due to a low density of measurements and hence there are many jumps and discontinuities in the sensor data. Unlike the multi-stage observer, the jumps and noise were not addressed when designing the high-gain observer. The estimation results of the multi-stage observer are therefore smoother and more reliable than the high-gain observer in the experiments.

In the first experiment shown in Fig. 8, a vehicle moves straight on a road perpendicular to the e-scooter's lane location. The orientation estimation of the vehicle remains at zero which agrees with the straight motion of the vehicle along the x-axis. The estimated velocity is also increasing suggesting that the vehicle is accelerating. In the second experiment shown in Fig. 9, a left-turning vehicle moves in front of the e-scooter. The estimate of the orientation angle for this vehicle changes from 180 degrees to 230 degrees as can be seen in Fig. 9. This result also agrees with the left-turning trajectory of vehicle 2. The smoother results of the multi-stage observer suggest that it is more reliable when it comes to speed and orientation estimation in the presence of measurement uncertainties.

We also compare the results of the high-gain and multistage observers with two cases of the Extended Kalman Filter (EKF) in Fig. 10 and Fig. 11. Both figures are based on the same experimental scenario in which a vehicle starts moving initially straight in the opposite direction to the e-scooter, and then turns left in front of the e-scooter, potentially creating some danger for the e-scooter rider. Fig. 10 shows the performance in which the EKF is designed assuming a low noise covariance matrix for sensor noise. In this case, the EKF has a very similar performance to the high-gain observer (especially in position and velocity estimation) as both observers use high values of feedback gain and rely heavily on the measurements. On the other hand, Fig. 11 shows the performance with the EKF having been designed with a higher noise covariance matrix. In this case, the performance of the EKF is seen to be very slow compared to the multistage nonlinear observer. Additionally, a major disadvantage of the EKF is that it might not be robust in the presence of model uncertainties in the nonlinear functions [23], while the multi-stage observer is guaranteed to be robust with the valid proofs presented in this paper. It is expected that the resulting estimates of the multi-stage observer always converge to the close neighborhood of the true state values when the basic assumptions (e. g. equations (6) and (7)) are followed. This is not necessarily true about the resulting estimates of the EKF even with perfectly chosen covariance matrices.

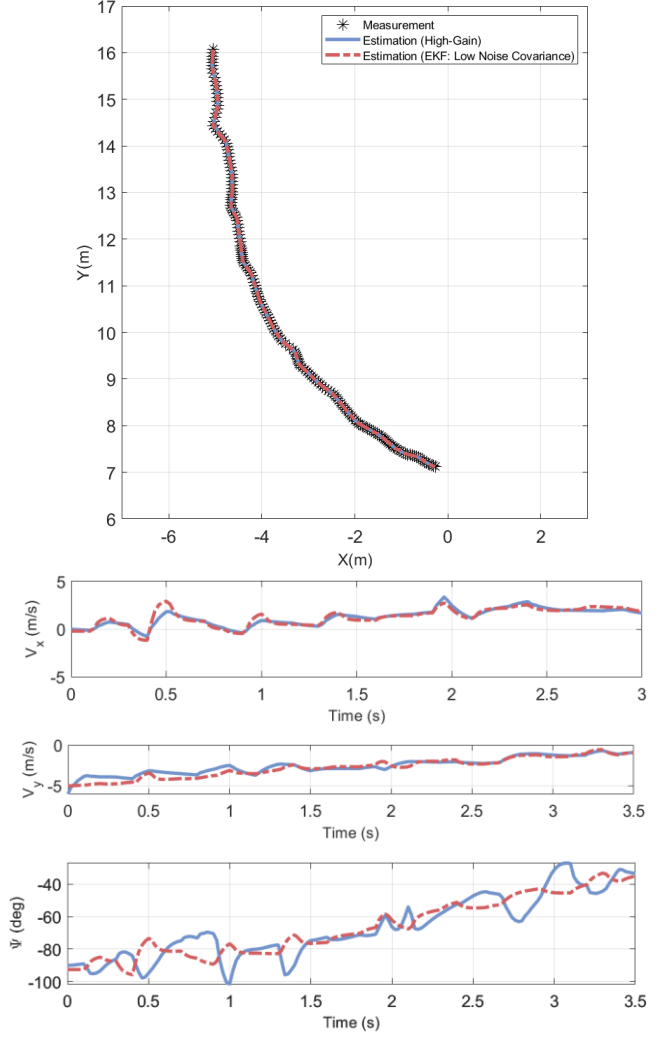


Fig. 10. Experimental Results of Scenario 3 in which the vehicle turns left in front of the e-scooter and eventually travels perpendicular to the escooter's direction. The EKF and the high-gain observer are compared.

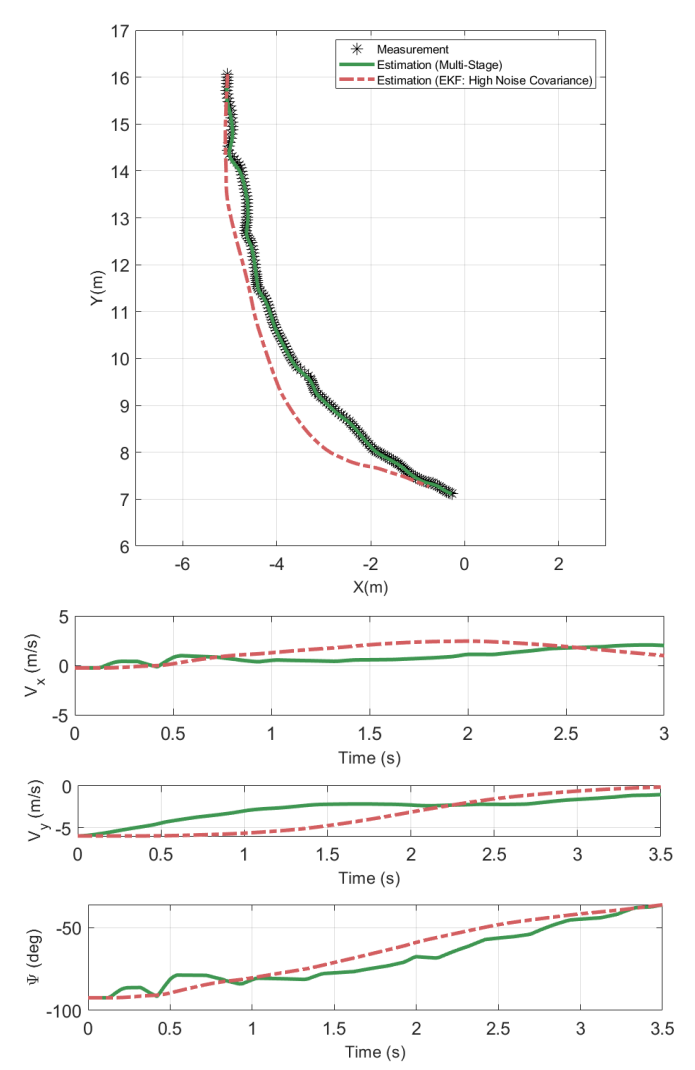


Fig. 11. Experimental Results of Scenario 3 in which the vehicle turns left in front of the e-scooter and eventually travels perpendicular to the e-scooter's direction. The EKF and the multi-stage observer are compared.

VI. CONCLUSION

A multi-stage estimation algorithm was developed in this paper for tracking the trajectories of other vehicles on the road. A kinematic model of the non-ego vehicle's motion was translated into three separate models for speed, orientation, and position. Three stable observers were then subsequently designed for these models which were all shown to be both stable and capable of rejecting the influence of uncertainties and disturbances.

The new estimation algorithm outperformed previous observers from the literature in simulations and experiments. Compared to the extended Kalman filter, the new observer provides smoother estimates and is also theoretically guaranteed to be asymptotically stable in the absence of disturbances. Compared to LMI-based nonlinear observers, the new observer theoretically supports variations in velocity and is shown to outperform the LMI observer in scenarios involving changes in velocity and steering. Compared to the high-gain nonlinear observer, the new observer requires smaller gains and outperforms the high-gain observer in terms

of smoother estimates for the jumpy RPLIDAR measurements.

A limitation of the developed multi-stage observer is that it still needs constraints on the allowable range of steering angles and slip angles. While the constraints in equations (8) and (9) allow for typical vehicle motions, they are violated under skidding on ice and other high-slip scenarios. Addressing these limitations will require stronger design methods for each of the three observers in this multi-stage algorithm.

The application of the developed observer was shown for an e-scooter protection system. Applications to other domains could also be evaluated in the future.

REFERENCES

- Grand View Research, "Electric Scooters Market Size, Share & Trends Analysis Report 2020 – 2030," Report ID: GVR-1-68038-196-2, February 2020.
- [2] Alai, H., Jeon, W., Alexander, L., and Rajamani, R., "Rear Vehicle Tracking on a Smart E-Scooter", In 2023 American Control Conference (ACC), 2023.
- [3] Y. K. Liew, C. P. J. Wee and J. H. Pek, "New peril on our roads: a retrospective study of electric scooter-related injuries", *Singapore Med J*, Vol. 61, No. 2, pp. 92-95, 2020.
- [4] Farley, K.X., Aizpuru, M., Wilson, J.M., Daly, C.A., Xerogeanes, J., Gottschalk, M.B. and Wagner, E.R., 2020. Estimated incidence of electric scooter injuries in the US from 2014 to 2019. JAMA network open, 3(8), pp.e2014500-e2014500.
- [5] Jianan Liu; Weiyi Xiong; Liping Bai; Yuxuan Xia; Tao Huang; Wanli Ouyang; Bing Zhu, "Deep Instance Segmentation With Automotive Radar Detection Points," *IEEE Transactions on Intelligent Vehicles*, Volume: 8, Issue: 1, pp. 84 94, January 2023.
- [6] Chengfeng Zhao; Chen Fu; John M. Dolan; Jun Wang, "L-Shape Fitting-Based Vehicle Pose Estimation and Tracking Using 3D-LiDAR," *IEEE Transactions on Intelligent Vehicles*, Volume: 6, Issue: 4, pp. 787-798, December 2021.
- [7] Jacob Velling Dueholm; Miklas Strøm Kristoffersen; Ravi Kumar Satzoda; Thomas Baltzer Moeslund; Mohan Manubhai Trivedi, "Trajectories and Maneuvers of Surrounding Vehicles With Panoramic Camera Arrays," *IEEE Transactions on Intelligent Vehicles*, Volume: 1, Issue: 2, pp. 203-214, June 2016.
- [8] Taohua Zhou; Junjie Chen; Yining Shi; Kun Jiang; Mengmeng Yang; Diange Yang, "Bridging the View Disparity Between Radar and Camera Features for Multi-Modal Fusion 3D Object Detection," *IEEE Transactions on Intelligent Vehicles*, Volume: 8, Issue: 2, pp. 1523-1535, February 2023.
- [9] Andras Palffy; Julian F. P. Kooij; Dariu M. Gavrila, "Detecting Darting Out Pedestrians With Occlusion Aware Sensor Fusion of Radar and Stereo Camera," *IEEE Transactions on Intelligent Vehicles*, Volume: 8, Issue: 2, pp. 1459-1472, February 2023.
- [10] Nachiket Deo; Akshay Rangesh; Mohan M. Trivedi, "How Would Surround Vehicles Move? A Unified Framework for Maneuver Classification and Motion Prediction," *IEEE Transactions on Intelligent Vehicles*, Volume: 3, Issue: 2, pp. 129-140, June 2018.
- [11] S. Danielsson, L. Petersson, and A. Eidehall, "Monte Carlo based Threat Assessment: Analysis and Improvements," Proceedings of the 2007 IEEE Intelligent Vehicles Symposium, IEEE, pp. 233-238, 2007.
- [12] Martin Treiber, Ansgar Hennecke, and Dirk Helbing, "Congested Traffic States in Empirical Observations and Microscopic Simulations," Phys. Rev. E 62, 1805 – Published 1 August 2000.
- [13] Jongyong Do; Kyoungseok Han; Seibum B. Choi, "Lane Change– Intention Inference and Trajectory Prediction of Surrounding Vehicles on Highways," *IEEE Transactions on Intelligent Vehicles*, Early Access, pp. 1 – 14, 2023.
- [14] Y. Bar-Shalom, X. R. Li, and T. Kirubarajan, Estimation with Applications to Tracking and Navigation: Theory Algorithms and Software. Hoboken, NJ, USA: Wiley, 2004.

- [15] Xu, P., Xiong, L., Zeng, D., Deng, Z. et al., "IMM-KF Algorithm for Multitarget Tracking of On-Road Vehicle," SAE Technical Paper 2020-01-0117, 2020, https://doi.org/10.4271/2020-01-0117.
- [16] Rajamani, R., Jeon, W., Movahedi, H. and Zemouche, A., 2020. On the need for switched-gain observers for non-monotonic nonlinear systems. Automatica, 114, p.108814.
- [17] Alai, H., Zemouche, A. and Rajamani, R., 2023, May. On Challenges in Coordinate Transformation for Using a High-Gain Multi-Output Nonlinear Observer. In 2023 American Control Conference (ACC).
- [18] Alai, H. and Rajamani, R., "Multi-Stage Estimation Algorithm for Vehicle Trajectory Tracking," In 2023 Modeling, Estimation, and Control Conference (MECC), 2023.
- [19] Rajamani, R., Vehicle dynamics and control. Springer, NY, 2011.
- [20] S. Boyd, L. El Ghaoui, E. Feron and V. Balakrishnan. "Linear Matrix Inequalities in System and Control Theory". SIAM Studies in Applied Mathematics. SIAM, Philadelphia, Pennsylvania, 1994.
- [21] Zemouche, A., Rajamani, R., Phanomchoeng, G., Boulkroune, B., Rafaralahy, H. and Zasadzinski, "Circle Criterion-based ℋ-∞ Observer Design for Lipschitz and Monotonic Nonlinear Systems – Enhanced LMI Conditions and Constructive Discussions," *Automatica*, 85, pp.412–425, 2017.
- [22] J. Lofberg, "YALMIP: A Toolbox for Modeling and Optimization in Matlab," Proceedings of the 2004 IEEE International Conference on Robotics and Automation, New Orleans, LA, USA, 2004.
- [23] H Movahedi, MA Figueroa-Santos, JB Siegel, AG Stefanopoulou and R. Rajamani, "Hybrid nonlinear observer for battery state-of-charge estimation using nonmonotonic force measurements," Advanced Control for Applications: Engineering and Industrial Systems, Vol. 2, No. 3, 2020.



Hamidreza Alai obtained his B.Sc. and M.Sc. degrees in mechanical engineering from the Sharif University of Technology and the University of Tehran, Tehran, Iran in 2016 and 2019, respectively. He is currently pursuing his Ph.D. degree at the University of Minnesota, Twin Cities, MN, USA. His research interests are in

state estimation, control, and mechanism design, including applications in intelligent transportation and robotic systems.



Rajesh Rajamani (Fellow, IEEE) obtained his M.S. and Ph.D. degrees from the University of California at Berkeley in 1991 and 1993 respectively and his B.Tech degree from the Indian Institute of Technology at Madras in 1989. Dr. Rajamani is currently the Benjamin Y.H. Liu-TSI Endowed

Professor of Mechanical Engineering and Associate Director of the Minnesota Robotics Institute at the University of Minnesota. His active research interests include sensing and estimation for smart mechanical systems.

Dr. Rajamani has co-authored over 180 journal papers and is a co-inventor on 14 granted patents. He is the author of the popular book "Vehicle Dynamics and Control" published by Springer. Dr. Rajamani has served as Chair of the IEEE Technical Committee on Automotive Control and is currently Senior Editor of the *IEEE Transactions on Intelligent Transportation Systems*. He is a Fellow of IEEE and ASME and has been a recipient of the CAREER award from the National Science Foundation, the Ralph Teetor Award from SAE, the Charles Stark Draper Award from ASME, the O. Hugo Schuck Award from the American Automatic Control Council, and a number of best paper awards from conferences

and journals. Several inventions from his laboratory have been commercialized through start-up ventures co-founded by industry executives. One of these companies, Innotronics, was recently recognized among the 35 Best University Start-Ups of 2016 by the US National Council of Entrepreneurial Tech Transfer.